Inducing or suppressing the anisotropy in multilayers based on CoFeB

Rafael Lopes Seeger,[1,*] Florian Millo,[2] Asma Mouhoub,[2] Grégoire de Loubens,[1] Aurélie Solignac,[1] and Thibaut Devolder[2]

[1]*SPEC, CEA, CNRS, Université Paris-Saclay, 91191 Gif-sur-Yvette, France*

[2]*Université Paris-Saclay, CNRS, Centre de Nanosciences et de Nanotechnologies, 91120 Palaiseau, France*

(Received 21 March 2023; accepted 15 May 2023; published 30 May 2023)

Controlling the uniaxial magnetic anisotropy is of practical interest for a wide variety of applications. We study $Co_{40}Fe_{40}B_{20}$ single films grown on various crystalline orientations of $LiNbO_3$ substrates and on oxidized silicon. We identify the annealing conditions that are appropriate to induce or suppress in-plane uniaxial anisotropy. Anisotropy fields can be increased by annealing up to 11 mT when using substrates with anisotropic surfaces. They can be decreased to below 1 mT when using isotropic surfaces. In the first case, the observed increase of the anisotropy originates from the biaxial strain in the film caused by the anisotropic thermal contraction of the substrate when back at room temperature after strain relaxation during annealing. In the second case, anisotropy is progressively removed by applying successive orthogonal fields that are assumed to progressively suppress any chemical ordering within the magnetic film. The method can be applied to CoFeB/Ru/CoFeB synthetic antiferromagnets, but the tuning of the anisotropy comes with a decrease of the interlayer exchange coupling and a drastic change in the exchange stiffness.

DOI: 10.1103/PhysRevMaterials.7.054409

I. INTRODUCTION

Controlling the anisotropy of a given magnetic material is very often required in applications of magnetism [1]. Amorphous metallic CoFeB films are widely used in spintronics, both when very soft properties are desired such as in flux guides [2] and, in contrast, when a well-defined uniaxial anisotropy is wanted such as in the free layers of magnetoresistive field sensors [3,4]. Depending on the targeted applications, the same material platform can even sometimes be used with opposite requirements for anisotropy. This is the case for artificial multiferroics composed of ferromagnetic films and piezoelectric layers. When intended, for instance, for energy harvesting, they require a well-defined anisotropy [5], while for racetrack applications isotropic properties are welcome [6]. Tailoring the uniaxial anisotropy, both *inducing* and *suppressing*, is thus an important challenge of technological interest.

Various knobs can be employed to tune the magnetic anisotropy. Interface engineering can be used in ultrathin films [7–9]. In bulk materials one can rely on either (i) some sort of chemical ordering [10] or (ii) the induction of anisotropic strain in magnetostrictive materials [11–13].

In the first case, one generally saturates the magnetization using a strong magnetic field and then provides thermal energy (hence atomic mobility) to let the structure of the material evolve towards a new state compatible with the desired magnetization orientation [14]. In metallic glass like CoFeB, the anisotropy is related to some degree of alignment of the boron atoms within the material, and this can be effectively tuned and reoriented by in-field annealing [10]. For the same reason, magnetic anisotropy can already be induced during deposition if done under an applied field [15].

The second case applies to only magnetostrictive materials. There, if an appropriate choice of the substrate influences the growth (e.g., epitaxy or strain relaxation), the resulting anisotropic strain leads to magnetic anisotropy [13]. This elastic coupling between the magnetic film and the substrate is systematically desired in SAW-FMR devices [16–18] and magnetoacoustics [19] when one harnesses the interaction between a surface acoustic wave (SAW) hosted by a piezoelectric substrate and the ferromagnetic resonance (FMR) of the magnetic film. Note that this situation fundamentally entails a dilemma when isotropic properties (meaning, often, stress-free layers) are desired in addition to a tight elastic coupling between the film and substrate. This dilemma is significant in the SAW-FMR of synthetic antiferromagnets (SAFs) since, in this case, a vanishing anisotropy is required for resonant coupling between the SAWs and the spin waves [20]. Unfortunately, it is difficult to obtain quasi-isotropic SAFs, and one typically is left with uniaxial anisotropy fields $\mu_0 H_k$ that remain above a couple of militeslas [21–24].

In this paper, we study how to tailor (increase or suppress) the in-plane magnetic anisotropy of magnetostrictive layers grown on piezoelectric substrates. We develop our method on $Co_{40}Fe_{40}B_{20}$ single-layer films grown on $LiNbO_3$ single crystals that are adequate for rf acoustical waves. We show that our method is applicable to SAFs. This paper is organized as follows. We initially quantify the uniaxial anisotropy in CoFeB and show how to control it through appropriate annealing and substrate choice. The surface orientation of $LiNbO_3$ strongly impacts how the annealing alters the anisotropy of the magnetic material. A well-designed procedure can lead to quasi-isotropic CoFeB layers and can be extended to CoFeB/Ru/CoFeB SAFs. However, spin wave spectroscopy

*rafael.lopesseeger@cea.fr.

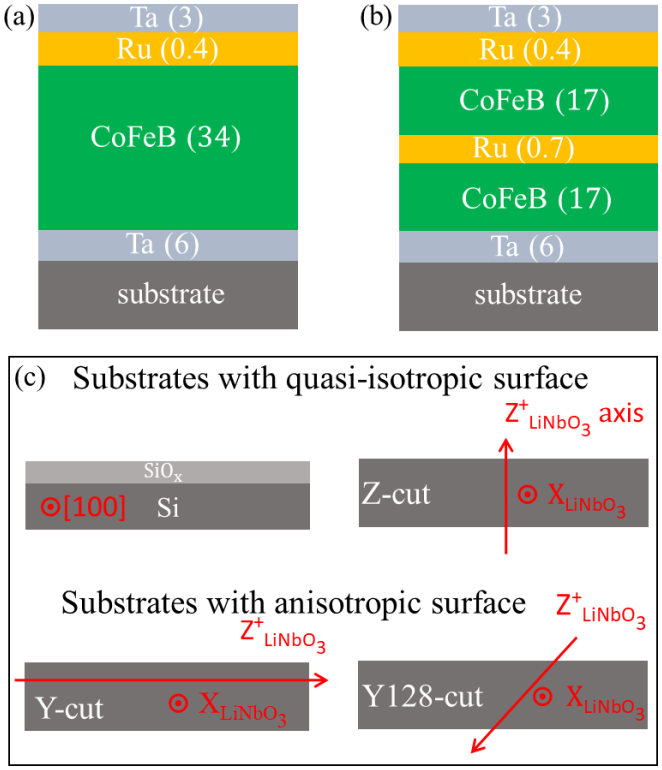

FIG. 1. Schematic illustration of the samples consisting of (a) a single CoFeB layer and (b) a CoFeB/Ru/CoFeB SAF. All thicknesses are given in nanometers. (c) Studied substrates. The red arrows indicate the direction of the ferroelectric order parameter (i.e., crystalline direction $Z^+_{LiNbO_3}$) around which a bulk substrate would exhibit rotational symmetry.

experiments show that the tailoring of the anisotropy of the SAF comes together with an evolution of the exchange stiffness and of the interlayer exchange coupling.

II. EXPERIMENTS

A. Films

Figure 1 depicts our material systems. The magnetic stacks are Ta(6, buffer)/CoFeB(34)/Ru(0.4)/Ta(3, cap) (abbreviated as single CoFeB) and Ta(6, buffer)/CoFeB (17)/Ru(0.7)/CoFeB(17)/Ru(0.4)/Ta(3, cap) (abbreviated as CoFeB/Ru/CoFeB SAF). All thicknesses are given in nanometers. The CoFeB layer was deposited from a $Co_{40}Fe_{40}B_{20}$ (at. %) target. The deposition is done at room temperature by dc magnetron sputtering at an argon pressure of 5×10^{-3} mbar and base pressure below 10^{-7} mbar. No intentional magnetic field is applied during growth. The Ru(0.4) layer is a sacrificial layer that avoids the resputtering of the top CoFeB layer caused by energetic bombardment of Ta atoms during sputtering of the capping layer. The thickness of the Ru(0.7) spacer of the SAF is chosen to maximize the interlayer exchange coupling [25].

B. Substrates

The depositions were done on several substrates ranging from naturally oxidized silicon wafers (referred to as Si/SiO_x) to $LiNbO_3$ single crystals with various surface orientations (Z, Y, and Y128 cut) [26]. Since the properties of the magnetic materials can be impacted by the stress induced by the underlying substrate [27], we place the substrates in two categories. The first category includes the substrates whose surface expands in a quasi-isotropic manner upon annealing. For the second category the thermal expansion is anisotropic at the surface, as illustrated in Fig. 1(c).

C. Postgrowth annealing conditions

In order to unravel the respective roles of substrate induced applied stress, applied field, and Boron diffusion onto the annealing-induced evolution of the magnetic properties, we annealed our material systems using four different procedures: (i) without any applied magnetic field, (ii) with 70 mT applied in a given direction in a one-step manner (we will see that the field direction, i.e., along or orthogonal to the initial anisotropy axis, does not influence the final result), (iii) with a 70 mT field applied in two successive steps (the sample is first annealed with a field oriented at some randomly chosen in-plane direction and then along its orthogonal direction), and (iv) in a 30 mT field rotating at 5 rpm in the sample plane.

The annealing temperature T ranges from 100 °C to 200 °C, above which systematic crystallization is expected for our boron content [28–31]. The annealing time is set to 4 min on a hot plate for procedures (i), (ii), and (iii). The annealing in rotating field [procedure (iv)] is done in vacuum for 10 h. In all cases the field is applied while ramping the temperature up and down and is strong enough to saturate the magnetization.

D. Magnetic characterizations

The magnetic characterization of samples was performed by vibrating sample magnetometry and vector network analyzer ferromagnetic resonance (VNA-FMR) [32]. An in-plane applied field $\mu_0 H_{ap}$ was used, and its direction θ [see Fig. 2(a)] was varied to access the sample's magnetic anisotropy. The resonance spectra (FMR absorption signal) are obtained by measuring the field dependence of the VNA transmission parameter $||S_{21}(H_{ap})|| - ||S_{21}(H = 0)||$, as plotted in Fig. 2(b). The resonance frequencies f_{res} (FMR for the single CoFeB or acoustical and optical resonances of the SAF) are defined from the maxima of absorption.

The θ dependence of the FMR of single CoFeB films were analyzed in the macrospin approximation using numerical energy minimization and subsequent application of the Smit-Beljers equation [33]. A fitting procedure allowed us to extract independently the values of the uniaxial anisotropy field H_k, the orientation of the easy axis, and the saturation magnetization M_s. Figure 2(c) illustrates this procedure when it is applied to a single CoFeB film grown on a Y128-cut substrate in the as-grown state. The orientation of the easy axis and the uniaxial character of the anisotropy are systematically consistent with the hysteresis loops.

The θ and H dependence of the acoustical, f_{acou}, and optical, f_{opt}, resonances of the SAF were analyzed in the full micromagnetic framework [34] following the method described in Ref. [25]. There, it was shown that the competition between the interlayer coupling J and the intralayer exchange

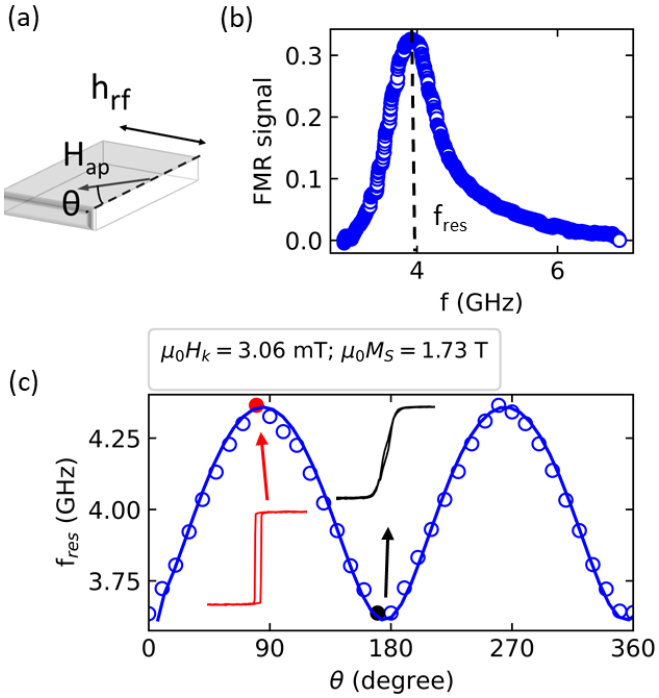

FIG. 2. Schematics of the experiment and representative results for a CoFeB single film on a Y128-cut substrate in the as-grown state. (a) VNA-FMR is conducted in an in-plane-oriented applied field of fixed magnitude $\mu_0 H_{ap} = 11.6$ mT and variable orientation $\theta \in [0°, 360°]$ with respect to the long axis of the sample. (b) Example of the VNA-FMR loss spectrum $||S_{21}(H_{ap})|| - ||S_{21}(H = 0)||$ and the definition of the resonance frequency f_{res}. (c) Symbols: experimental θ dependence of f_{res}. Line: fit within the macrospin model with uniaxial anisotropy field H_k and magnetization as free parameters. Insets: experimental hysteresis loops obtained along the easy axis (red curve, $\theta \cong 90°$) and hard xis (black curve, $\theta \cong 180°$).

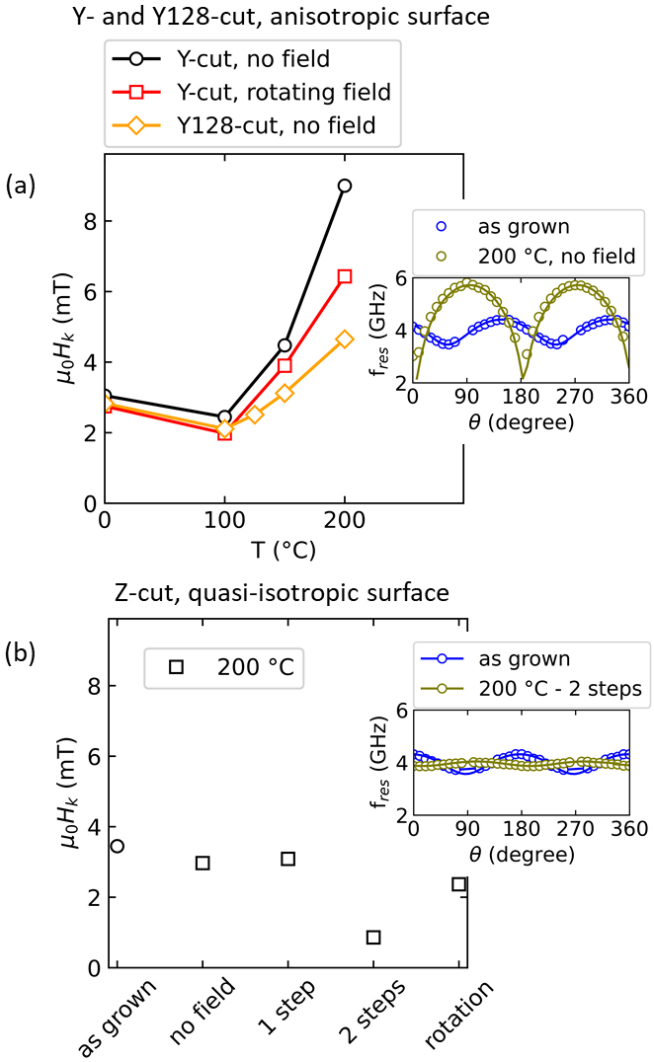

FIG. 3. (a) Anisotropy field H_k dependence on the annealing temperature T as measured for single CoFeB grown on Y-cut $LiNbO_3$ as an example of the effect of annealing on a substrate with an anisotropic surface. (b) Representative H_k dependence for samples subjected to various annealing procedures with $T = 200\,°C$, as measured for single CoFeB grown on Z-cut $LiNbO_3$, a substrate with a quasi-isotropic surface. Insets in (a) and (b) are the representative θ dependence of f_{res} before and after annealing. The line is a fit to the experimental data (see discussion in the text).

stiffness A_{ex} results in the existence of a gradient of the magnetization orientation in the growth direction. This gradient renders the curvature of $f_{opt}(\theta)$ near $H = 0$ very sensitive to the ratio of A_{ex} and J, which can thus be deduced reliably. A fitting procedure of $f_{acou}(\theta)$ can then be used to extract the anisotropy fields, which are assumed to be exactly the same for the two magnetic layers of the SAF.

III. EVOLUTION OF THE IN-PLANE MAGNETIC ANISOTROPY UPON ANNEALING

A. Results

The main features of the evolution of the magnetic anisotropy upon annealing are illustrated in Fig. 3 and compiled in Table I. An annealing temperature above 100 °C appears to be necessary to observe an evolution of the magnetic properties. The atomic mobility within the CoFeB films is likely insufficient below this temperature. For larger annealing temperatures, the magnetic anisotropy evolves in very different ways depending on whether the substrate has an isotropic or anisotropic surface and also on the field applied.

When working on substrates with anisotropic surfaces (Y-cut and Y128-cut $LiNbO_3$), the annealing substantially increases the anisotropy [see Fig. 3(a)]. The inset compares the angular dependence of the FMR of a CoFeB film on a Y-cut $LiNbO_3$ substrate before and after a 200 °C field-free annealing. Annealing increases the anisotropy field $\mu_0 H_k$ from 3.05 to 9.00 mT. This comes with a reorientation of the hard axis towards X_{LiNbO_3} (i.e., $\theta = 0°$ in our convention). The Y128-cut samples follow a similar trend but with a lower increase of the anisotropy. As soon as the anisotropy increases, the hard axis also reorients towards the X_{LiNbO_3} axis, and the easy axis reorients towards the in-plane projection of the Z_{LiNbO_3} axis. When working on these substrates with anisotropic surfaces, the magnetic field applied (or not) during the annealing has a minor influence on the evolution of the magnetic anisotropy.

Conversely, the anisotropy can be reduced for the films grown on substrates with quasi-isotropic surfaces: Z-cut $LiNbO_3$ and oxidized silicon. The inset in Fig. 3(b) shows the angular dependence of the FMR before and after a two-step annealing procedure in the case of a Z-cut $LiNbO_3$ substrate. This two-step annealing lowers the anisotropy down to 0.6 mT. Notably, the rate of decrease of the anisotropy depends strongly on the field sequence used during annealing, and the hard axis systematically ends perpendicular to the field applied during the last annealing step.

B. Physical origins of the evolution of anisotropy

The previous results can be discussed by considering two thermodynamic phenomena: (i) the interplay between magnetoelasticity and anisotropic strain and (ii) the chemical ordering within the magnetic material. We recall that for the annealing temperatures studied here, no crystallization of the CoFeB layer is expected. Let us first discuss the magnetoelastic scenario.

1. Magnetoelastic scenario

With annealing above $T_a > 100\,^{\circ}\mathrm{C}$, the atoms within the CoFeB film acquire some mobility, as observed in other soft magnetic materials [10]. Being amorphous, the glassy CoFeB film slowly flows, such that after a sufficient delay, it reaches a relaxed (stress-free) state at the annealing temperature. Cooling (defined as $\mathrm{RT} - T_a = \delta T < 0$) to room temperature (RT) suddenly quenches any atomic mobility while triggering a thermal contraction. Since the CoFeB film is clamped by the much thicker single-crystal substrate, the in-plane strain ε of the substrate is imposed on the magnetic film. The natural contraction of a hypothetically freestanding CoFeB film would be isotropic (its thermal expansion coefficient β is isotropic). That of the $LiNbO_3$ substrate is not: the thermal expansion coefficient in the X_{LiNbO_3} direction is stronger than in the other direction of the substrate plane [27]. As a result the strain $\bar{\bar{\varepsilon}}$ within the CoFeB at RT is biaxial and more compressive in the X_{LiNbO_3} direction. Defining x and y as the two directions of the surface of the substrate with $x \parallel X_{LiNbO_3}$ [see Fig. 1(c)], we have

$$\varepsilon_{xx} = \beta_x \delta T < 0, \quad \varepsilon_{yy} = \beta_y \delta T < 0. \tag{1}$$

Whatever the substrate cut, the largest deformation is always along X_{LiNbO_3} (see Ref. [27]). We have $\beta_x > \beta_y$ for both the Y-cut case and the Y128-cut case. As CoFeB essentially has a free surface, its stress is purely biaxial, such that there is no shear strain (i.e., $\varepsilon_{xy} = 0$).

This biaxial strain generates magnetic anisotropy of CoFeB. Indeed, for an in-plane magnetized film, the magnetoelastic energy is $E_{me} = B_1(m_x^2\varepsilon_{xx} + m_y^2\varepsilon_{yy}) + 2B_2 m_x m_y \varepsilon_{xy}$, where B_1 and B_2 are the usual magnetoelastic coefficients. In amorphous materials, they reduce to $-\frac{3}{2}\lambda E_{Young}$, which amounts to $-7.6\,\mathrm{MJ/m^3}$ with the magnetostriction coefficient $\lambda = 27$ ppm for $Co_{40}Fe_{40}B_{20}$ from Ref. [35] and Young's modulus $E_{Young} = 187$ GPa from Ref. [36]. Note that $\lambda > 0$, meaning tensile strain lowers the energy. With the CoFeB film being more compressed in the X direction than in other directions, X_{LiNbO_3} will become the hard axis. Using the conservation of the magnetization norm and $\varepsilon_{xy} = 0$, we can rewrite this energy in the form of an effective uniaxial anisotropy:

$$E_{me} = B_1 m_x^2 (\varepsilon_{xx} - \varepsilon_{yy}) \tag{2}$$

with a magnetoelastic effective anisotropy field of

$$\mu_0 H_k^{mel} = \frac{2B_1}{M_s}(\beta_x - \beta_y)\delta T, \tag{3}$$

which is predicted to be linear with the annealing temperature, which bears some similarity to the experimental results [see Fig. 3(a)] above $T_a = 100\,^{\circ}\mathrm{C}$.

Using the data in Table II with $\delta T = -180$ K, Eq. (3) predicts $\mu_0 H_k^{mel} = 5.5$ mT for the Y128-cut case and $\mu_0 H_k^{mel} = 13.7$ mT for the Y-cut case, with hard axes along X_{LiNbO_3} in both cases. This magnetoelastic contribution dominates any other contribution to the uniaxial anisotropy, including the one present in the as-grown state and those possibly related to the magnetic field applied during the annealing. This correlates with our finding on the minor influence of the field applied during the annealing of Y- and Y128-cut samples. Note that the predicted values of the anisotropy field H_k^{mel} are slightly larger than our experimental findings. This may indicate that the stress release is incomplete during the annealing or that the magnetostriction coefficient in the literature [35] is overestimated.

Another conclusion of our study concerns the evolution of the magnetization M_s upon annealing (Table I). There is little evolution for the Si/SiO_x case but a substantial increase otherwise. For our nominal boron concentration, bulk crystallization and stress-induced bulk crystallization are not supposed to occur at our annealing temperatures [37] and can therefore not be invoked for the observed increase of the magnetization. However, some compression-induced diffusion of the boron atoms out of the magnetic films may start to occur, thereby reducing the boron concentration. The corresponding densification is generally associated with an increase of the magnetization [38]. We indeed observe that the increase of the magnetization after the 200 °C annealings seems to correlate with the amount of compression (see Tables I and II).

This anisotropic strain-induced scenario is effective only for substrates with anisotropic thermal expansion like Y-cut and Y128-cut $LiNbO_3$. Another scenario must thus be invoked for the Z cut of $LiNbO_3$ and the oxidized silicon cases.

2. Chemical order scenario

In many magnetic alloys, it is routinely observed that annealing in a magnetic field induces a preferred direction of magnetization [7,14]. A plausible model often invoked to explain this mechanism is the migration of atoms on a local scale in such a way as to favor magnetization in a given direction. At annealing temperatures leading to some atomic mobility, some atom pairs orient themselves relative to the direction of magnetization set by the field to decrease their magnetic anisotropy energy. Cooling to a temperature where atomic diffusion gets quenched, the anisotropy axis remains along the direction it acquired during annealing. Metalloids like boron play an important role in this process thanks to their high mobility and chemical interaction with transition metals [10]. In a metallic glass like CoFeB the applied field drives the anisotropic distribution of atoms pairs among Co,

TABLE I. Summary of the material parameters obtained from fitting of single CoFeB subjected to different thermal treatments. "Variable" means that the value of the anisotropy field and its orientation depend on the sample position within the deposition machine; the evolution of $\mu_0 H_k$ is, however, taken for a consistent sample position.

Substrate	Thermal treatment	$\mu_0 H_k$ (mT), ±5%	Hard axis	$\mu_0 M_s$ (T), ±0.01
		Substrates with quasi-isotropic surface		
SiO_x	as grown	3.0	variable	1.70
	200 °C, $H = 0$	3.1	variable	1.72
	200 °C, rotating H	1.5	variable	1.71
	200 °C two-step H	0.9	⊥ to last field	1.76
Z	as grown	2.2	variable	1.70
	200 °C, $H = 0$	2.8	variable	1.71
	200 °C, rotating H	2.4	variable	1.82
	200 °C two-step H	0.6	⊥ to last field	1.70
		Substrates with an anisotropic surface		
Y128	as grown	3.1	variable	1.77
	200 °C, $H = 0$	4.3	∥ X_{LiNbO_3}	1.87
Y	as grown	3.0	variable	1.70
	200 °C, $H = 0$	9.0	∥ X_{LiNbO_3}	2.00
	200 °C, rotating H	6.4	∥ X_{LiNbO_3}	2.00
	200 °C two-step H	11.4	∥ X_{LiNbO_3}	2.00

Fe, and B, and this mechanism is active at the timescales used for annealing for the temperatures considered here [10]. This process is generally used to induce anisotropy, using a *fixed* field orientation and a *long* annealing.

However, it is important to figure out that the material evolution is a thermodynamical process. In our two-step process, during the first annealing step, the field-induced (energy-minimization-driven) chemical ordering process competes with a temperature-induced (random, entropy-driven) disordering trend. This competition leads to the slow formation of uniaxial anisotropy. During the subsequent annealing step, the magnetic field orientation is different. As a result, the entropy-driven and energy-driven thermodynamical forces both tend to destroy the previously favored chemical order, and therefore, they act together to reduce the anisotropy. Because of this coincidence of the two thermodynamical forces at play, this destruction of the previously set anisotropy is a fast process. The building up of any uniaxial anisotropy along a new field direction is a much slower process. In practice, it is not seen at the timescales used in our annealings.

This explains how one can progressively reduce the anisotropy by applying successive orthogonal fields during annealing when there is no magnetoelastic contribution at play. Each annealing step with a new field direction statistically breaks pair alignments, which results in a progressive randomization of the chemical ordering within the magnetic film and thus a decrease of the anisotropy. The effect of annealing under a rotating field is qualitatively similar to two-step annealing. Note, however, that their relative efficiency depends on the characteristic timescales of atomic diffusion versus the field rotation period, explaining the difference in the final anisotropy strength depending on the annealing process.

To summarize the discussion so far, the findings presented in Fig. 3 indicate that, with regard to the substrate, different contributions to the uniaxial anisotropy of CoFeB may arise. For surface substrates with anisotropic thermal expansion (Y-cut and Y128-cut $LiNbO_3$), the anisotropy is controlled by anisotropic strain, while for quasi-isotropic surface substrates (Si/SiO_x and Z-cut $LiNbO_3$), the anisotropy is controlled by the chemical ordering favored or broken by the sequence of applied magnetic fields.

IV. APPLICABILITY TO SYNTHETIC ANTIFERROMAGNETS

It is important to investigate whether the conclusions previously established for single CoFeB films can be extended to multilayers. In particular, let us see whether one can obtain isotropic CoFeB/Ru/CoFeB SAFs when they are grown on quasi-isotropic substrates. Figure 4 shows the results for a SAF grown on Si/SiO_x in the as-grown state and after annealing in a rotating field. The two lowest-order spin wave modes can be detected, the acoustical (f_{acou}) and optical (f_{opt}) modes. The value of f_{acou} at low field is known to be very

TABLE II. Thermal expansion coefficients in the two directions of the surface plane, in units of $10^{-5}/°C$.

Surface	β in the first direction	β along a perpendicular direction
Y-cut	along X_{LiNbO_3}: $\beta_1 = 1.5$	along X_{LiNbO_3}: $\beta_3 = 0.7$
Y128-cut	along X_{LiNbO_3}: $\beta_1 = 1.5$	$\beta_1 \sin^2(128) + \beta_3 \cos^2(128) = 1.2$
Z-cut	along X_{LiNbO_3}: $\beta_1 = 1.5$	along X_{LiNbO_3}: $\beta_1 = 1.5$
Si[001]	along [100]: 0.468	along [010]: 0.468

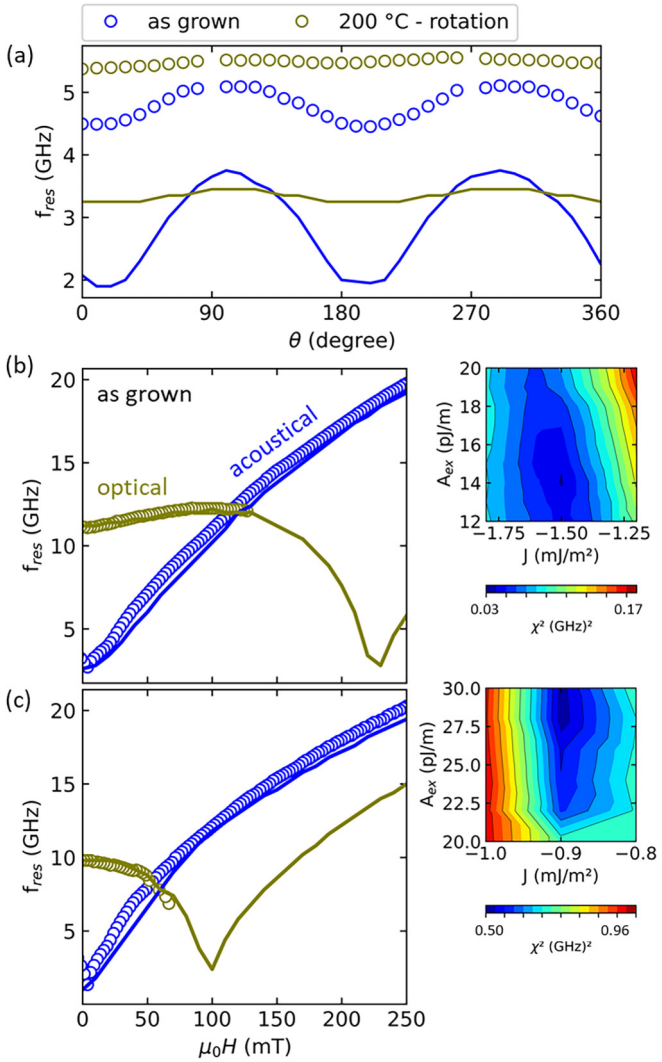

FIG. 4. Effect of annealing in a rotating field for CoFeB/Ru/CoFeB SAFs grown on Si/SiO_x. (a) θ dependence of f_{res} before and after annealing. Symbols are experimental data. The lines show the calculated dependences from micromagnetic simulations [34] using magnetic parameters fitted from the broadband VNA-FMR characterization of the acoustical and optical modes shown in (b) in the as-grown state and in (c) after annealing. Insets show color maps of the distance between the experimental and simulated spin wave frequencies used to determine A_{ex} and J.

sensitive on the anisotropy field [39]. The θ dependence of f_{acou} [Fig. 4(a)] clearly indicates that the annealing procedure defined for the single layer films also succeeds in suppressing the anisotropy of the SAF grown on Si/SiO_x. As will be explained later, we can give only a semiquantitative measurement of the anisotropy field $\mu_0 H_k$ of the SAF, but its reduction (see Table III) is almost complete. The same trend is observed when the growth is performed on Z-cut $LiNbO_3$; see Table III for results in the as-grown state and after a two-step annealing.

However, this quasisuppression of the anisotropy is accompanied by an evolution of the other magnetic properties. This can be seen by comparing the frequencies of the experimental and simulated modes using the methodology defined in Ref. [25]. Indeed, the value of f_{opt} at $H = 0$ is essentially set by the interlayer coupling J. Annealing obviously reduces it [compare Figs. 4(b) and 4(c)]. In addition, the curvature of f_{opt} versus H is very sensitive to the ratio $\frac{A_{ex}}{J}$: annealing obviously strongly affects this ratio.

TABLE III. Material parameters of the synthetic antiferromagnet before and after annealing. The processes employed for SiO_x and Z_{LiNbO_3} substrates are rotating field and two-step annealing, respectively.

Substrate	$\mu_0 H_k$ (mT)	$\mu_0 M_s$ (T)	J (mJ/m^2)	A_{ex} (pJ/m)
SiO_x, as grown	4.4	1.70	−1.5	14.5
SiO_x, 200 °C	0.8	1.71	−0.9	28.3
Z_{LiNbO_3}, as grown	3.8	1.70	−1.7	15.5
Z_{LiNbO_3}, 200 °C	0.5	1.70	−1.1	21

The values of A_{ex} and J that best fit the experimental data for Si/SiO_x and Z-cut $LiNbO_3$ substrates are listed in Table III. The experiment-to-micromagnetics agreement is excellent except in the small field region for the acoustical spin wave, where micromagnetics systematically underestimates the frequency of the acoustical mode [Figs. 4(b) and 4(c)]. The same difficulty arises when attempting to account for the θ dependence of f_{acou} with micromagnetic simulations, as shown in Fig. 4(a). The reason for this disagreement was not identified, but we believe that it may arise from a gradient of the magnetic properties in the growth direction which is not taken into account in the simulations. For this reason, we can give only a semiquantitative measurement of the anisotropy field $\mu_0 H_k$. The anisotropy values in Table III are deduced from the sole value of f_{acou} at zero field.

Upon annealing, J reduces from -1.5 to -0.9 mJ/m^2, as observed for our SAF grown on Si/SiO_x. The atomic mobility enabled by the annealing probably reduces the sharpness of the interfaces of the Ru spacer, thereby decreasing J. The evolution of the local order within the CoFeB material is also evident from the evolution of its exchange stiffness A_{ex}, which undergoes a very substantial increase from 14.5 to 28.3 pJ/m upon annealing. It is noteworthy that the as-grown value of A_{ex} is comparable to literature values in the amorphous state for our composition, which are found to be [25,40,41] in the range from 10 to 14 pJ/m. The exchange stiffness is also known to increase substantially when the layer becomes either crystalline or simply more dense [38].

V. CONCLUSION

We have studied the impact of annealing on the magnetic properties of CoFeB films and synthetic antiferromagnets. We studied in-plane uniaxial anisotropy in CoFeB single films by performing various in-field thermal treatments for films grown on different substrates. The anisotropy field of CoFeB can be increased when the annealing is performed on samples grown on substrates whose surfaces have an anisotropic thermal expansion. In this case the likely scenario is a full stress relaxation occurring during the annealing, followed by the creation of biaxial strain in CoFeB upon cooling, which induces a strong magnetoelastic anisotropy. Anisotropy fields up to 11 mT can be induced when extremely

anisotropic substrates like Y-cut $LiNbO_3$ are used. Conversely, the anisotropy field can be decreased to below 1 mT when using substrates whose surface is quasi-isotropic. In this case the anisotropy is controlled by the history of the magnetic field applied during annealing. In particular, sequences of orthogonal fields are very efficient in suppressing the in-plane anisotropy. This method was applied to obtain isotropic CoFeB/Ru/CoFeB synthetic antiferromagnets; however, the annealing also affects the exchange interactions within the stack.

ACKNOWLEDGMENTS

We acknowledge discussions with S. Margueron, A. Bartasyte, and C. Chappert. This work was supported by a public grant overseen by the French National Research Agency (ANR) as part of the "Investissements d'Avenir" program (Labex NanoSaclay, Reference No. ANR-10-LABX-0035, project SPICY). R.L.S. and F.M. acknowledge the French National Research Agency (ANR) under Contract No. ANR-20-CE24-0025 (MAXSAW).

[1] A. Hirohata, K. Yamada, Y. Nakatani, I.-L. Prejbeanu, B. Diény, P. Pirro, and B. Hillebrands, Review on spintronics: Principles and device applications, J. Magn. Magn. Mater. **509**, 166711 (2020).

[2] N. Smith, F. Jeffers, and J. Freeman, A high-sensitivity magnetoresistive magnetometer, J. Appl. Phys. **69**, 5082 (1991).

[3] K. Hayakawa, S. Kanai, T. Funatsu, J. Igarashi, B. Jinnai, W. A. Borders, H. Ohno, and S. Fukami, Nanosecond Random Telegraph Noise in In-Plane Magnetic Tunnel Junctions, Phys. Rev. Lett. **126**, 117202 (2021).

[4] A. Deka, B. Rana, R. Anami, K. Miura, H. Takahashi, Y. Otani, and Y. Fukuma, Electric field induced parametric excitation of exchange magnons in a CoFeB/MgO junction, Phys. Rev. Res. **4**, 023139 (2022).

[5] K. Roy, S. Bandyopadhyay, and J. Atulasimha, Hybrid spintronics and straintronics: A magnetic technology for ultra low energy computing and signal processing, Appl. Phys. Lett. **99**, 063108 (2011).

[6] N. Lei, T. Devolder, G. Agnus, P. Aubert, L. Daniel, J.-V. Kim, W. Zhao, T. Trypiniotis, R. P. Cowburn, C. Chappert, D. Ravelosona, and P. Lecoeur, Strain-controlled magnetic domain wall propagation in hybrid piezoelectric/ferromagnetic structures, Nat. Commun. **4**, 1378 (2013).

[7] R. C. O'Handley, *Modern Magnetic Materials: Principles and Applications* (Wiley-Interscience, 1999).

[8] C. Chappert, H. Bernas, J. Ferré, V. Kottler, J.-P. Jamet, Y. Chen, E. Cambril, T. Devolder, F. Rousseaux, V. Mathet, and H. Launois, Planar patterned magnetic media obtained by ion irradiation, Science **280**, 1919 (1998).

[9] A. Deka, B. Rana, R. Anami, K. Miura, H. Takahashi, Y. Otani, and Y. Fukuma, Electric-field control of interfacial in-plane magnetic anisotropy in CoFeB/MgO junctions, Phys. Rev. B **101**, 174405 (2020).

[10] E. van de Riet, W. Klaassens, and F. Roozeboom, On the origin of the uniaxial anisotropy in nanocrystalline soft-magnetic materials, J. Appl. Phys. **81**, 806 (1997).

[11] G. A. Lebedev, B. Viala, T. Lafont, D. I. Zakharov, O. Cugat, and J. Delamare, Converse magnetoelectric effect dependence with CoFeB composition in ferromagnetic/piezoelectric composites, J. Appl. Phys. **111**, 07C725 (2012).

[12] V. B. Naik, H. Meng, J. X. Xiao, R. S. Liu, A. Kumar, K. Y. Zeng, P. Luo, and S. Yap, Effect of electric-field on the perpendicular magnetic anisotropy and strain properties in CoFeB/MgO magnetic tunnel junctions, Appl. Phys. Lett. **105**, 052403 (2014).

[13] S. A. Mathews and J. Prestigiacomo, Controlling magnetic anisotropy in nickel films on $LiNbO_3$, J. Magn. Magn. Mater. **566**, 170314 (2023).

[14] S. Chikazumi, *Physics of Ferromagnetism*, International Series of Monographs on Physics (Oxford University Press, Oxford, 2009).

[15] F. G. West, Uniaxial anisotropy due to magnetoelastic energy in constrained polycrystalline films, J. Appl. Phys. **35**, 1827 (1964).

[16] M. Weiler, L. Dreher, C. Heeg, H. Huebl, R. Gross, M. S. Brandt, and S. T. B. Goennenwein, Elastically Driven Ferromagnetic Resonance in Nickel Thin Films, Phys. Rev. Lett. **106**, 117601 (2011).

[17] P. Kuszewski, J.-Y. Duquesne, L. Becerra, A. Lemaître, S. Vincent, S. Majrab, F. Margaillan, C. Gourdon, and L. Thevenard, Optical Probing of Rayleigh Wave Driven Magnetoacoustic Resonance, Phys. Rev. Appl. **10**, 034036 (2018).

[18] P. Rovillain, J.-Y. Duquesne, L. Christienne, M. Eddrief, M. G. Pini, A. Rettori, S. Tacchi, and M. Marangolo, Impact of Spin-Wave Dispersion on Surface-Acoustic-Wave Velocity, Phys. Rev. Appl. **18**, 064043 (2022).

[19] M. Küß, M. Albrecht, and M. Weiler, Chiral magnetoacoustics, Front. Phys. **10**, 981257 (2022).

[20] R. Verba, V. Tiberkevich, and A. Slavin, Wide-Band Nonreciprocity of Surface Acoustic Waves Induced by Magnetoelastic Coupling with a Synthetic Antiferromagnet, Phys. Rev. Appl. **12**, 054061 (2019).

[21] A. T. Hindmarch, C. J. Kinane, M. MacKenzie, J. N. Chapman, M. Henini, D. Taylor, D. A. Arena, J. Dvorak, B. J. Hickey, and C. H. Marrows, Interface Induced Uniaxial Magnetic Anisotropy in Amorphous CoFeB Films on AlGaAs(001), Phys. Rev. Lett. **100**, 117201 (2008).

[22] A. W. Rushforth, E. De Ranieri, J. Zemen, J. Wunderlich, K. W. Edmonds, C. S. King, E. Ahmad, R. P. Campion, C. T. Foxon, B. L. Gallagher, K. Výborný, J. Kučera, and T. Jungwirth, Voltage control of magnetocrystalline anisotropy in ferromagnetic-semiconductor-piezoelectric hybrid structures, Phys. Rev. B **78**, 085314 (2008).

[23] M. González-Guerrero, J. L. Prieto, D. Ciudad, P. Sánchez, and C. Aroca, Engineering the magnetic properties of amorphous $(Fe_{80}Co_{20})_{80}B_{20}$ with multilayers of variable anisotropy direction, Appl. Phys. Lett. **90**, 162501 (2007).

[24] H. W. Chang, F. T. Yuan, D. Y. Lin, D. H. Tseng, W. C. Chang, Y. S. Chen, and J. G. Lin, Large stress-induced anisotropy in soft magnetic films for synthetic spin valves, Appl. Phys. Lett. **119**, 242402 (2021).

[25] A. Mouhoub, F. Millo, C. Chappert, J.-V. Kim, J. Létang, A. Solignac, and T. Devolder, Exchange energies in CoFeB/Ru/CoFeB synthetic antiferromagnets, Phys. Rev. Mater. **7**, 044404 (2023)..

[26] J. Kushibiki, I. Takanaga, S. Komatsuzaki, and T. Ujiie, Chemical composition dependences of the acoustical physical constants of $LiNbO_3$ and $LiTaO_3$ single crystals, J. Appl. Phys. **91**, 6341 (2002).

[27] A. Bartasyte, V. Plausinaitiene, A. Abrutis, T. Murauskas, P. Boulet, S. Margueron, J. Gleize, S. Robert, V. Kubilius, and Z. Saltyte, Residual stresses and clamped thermal expansion in $LiNbO_3$ and $LiTaO_3$ thin films, Appl. Phys. Lett. **101**, 122902 (2012).

[28] C. Y. You, T. Ohkubo, Y. K. Takahashi, and K. Hono, Boron segregation in crystallized MgO/amorphous-$Co_{40}Fe_{40}B_{20}$ thin films, J. Appl. Phys. **104**, 033517 (2008).

[29] A. Conca, E. Th. Papaioannou, S. Klingler, J. Greser, T. Sebastian, B. Leven, J. Lösch, and B. Hillebrands, Annealing influence on the gilbert damping parameter and the exchange constant of CoFeB thin films, Appl. Phys. Lett. **104**, 182407 (2014).

[30] T. Devolder, J.-V. Kim, J. Swerts, S. Couet, S. Rao, W. Kim, S. Mertens, G. Kar, and V. Nikitin, Material developments and domain wall-based nanosecond-scale switching process in perpendicularly magnetized STT-MRAM cells, IEEE Trans. Magn. **54**, 1 (2018).

[31] K. Sriram, J. Pala, R. Mondal, B. Paikaray, K. Jain, G. A. Basheed, A. Haldar, and C. Murapaka, Effect of annealing on magnetization reversal and spin dynamics in $Co_{40}Fe_{40}B_{20}$ thin films, J. Supercond. Novel Magn. **36**, 155 (2022).

[32] C. Bilzer, T. Devolder, P. Crozat, C. Chappert, S. Cardoso, and P. P. Freitas, Vector network analyzer ferromagnetic resonance of thin films on coplanar waveguides: Comparison of different evaluation methods, J. Appl. Phys. **101**, 074505 (2007).

[33] J. Smit and H. G. Beljers, Ferromagnetic resonance absorption in $BaFe_{12}O_{19}$, a highly anisotropic crystal, Philips Res. Rep. **10**, 113 (1955).

[34] A. Vansteenkiste, J. Leliaert, M. Dvornik, M. Helsen, F. Garcia-Sanchez, and B. V. Waeyenberge, The design and verification of MuMax3, AIP Adv. **4**, 107133 (2014).

[35] G. Masciocchi, M. Fattouhi, A. Kehlberger, L. Lopez-Diaz, M.-A. Syskaki, and M. Kläui, Strain-controlled domain wall injection into nanowires for sensor applications, J. Appl. Phys. **130**, 183903 (2021).

[36] R.-C. Peng, J.-M. Hu, K. Momeni, J.-J. Wang, L.-Q. Chen, and C.-W. Nan, Fast 180° magnetization switching in a strain-mediated multiferroic heterostructure driven by a voltage, Sci. Rep. **6**, 27561 (2016).

[37] M. M. Trexler and N. N. Thadhani, Mechanical properties of bulk metallic glasses, Prog. Mater. Sci. **55**, 759 (2010).

[38] J.-S. Kim, G. Kim, J. Jung, K. Jung, J. Cho, W.-Y. Kim, and C.-Y. You, Control of crystallization and magnetic properties of CoFeB by boron concentration, Sci. Rep. **12**, 4549 (2022).

[39] T. Devolder and K. Ito, Spin torque switching and scaling in synthetic antiferromagnet free layers with in-plane magnetization, J. Appl. Phys. **111**, 123914 (2012).

[40] J. Cho, J. Jung, K.-E. Kim, S.-I. Kim, S.-Y. Park, M.-H. Jung, and C.-Y. You, Effects of sputtering Ar gas pressure in the exchange stiffness constant of $Co_{40}Fe_{40}B_{20}$ thin films, J. Magn. Magn. Mater. **339**, 36 (2013).

[41] G.-M. Choi, Exchange stiffness and damping constants of spin waves in CoFeB films, J. Magn. Magn. Mater. **516**, 167335 (2020).